

Effects of Surfactant and Polymer on the Morphology of Advanced Nanomaterials in Aqueous Solution

Shael Ahmed AL-Tabaiti¹, Maqsood Ahmad Malik¹, Abdulrahman A. O. Al-Youbi¹, Zaheer Khan^{2,*}, Javed Ijaz Hussain²

¹Department of Chemistry, Faculty of Science, King Abdulaziz University, P.O. Box 80203, Jeddah 21413, Saudi Arabia.

²Nano-science research lab, Department of Chemistry, Jamia Millia Islamia (Central University), New Delhi-110025, India.

*E-mail: drkhanchem@yahoo.co.in

Received: 17 September 2012 / Accepted: 28 November 2012 / Published: 1 January 2013

The sculpturing effects of cetyltrimethylammonium bromide and poly(vinyl)alcohol on the shape transformation of silver nano-particles are presented. It is a simple process of recent interest for obtaining silver nano-rods, spherical and hexagonal nano-plates in the thiosulphate reduction of Ag⁺ ions with or without stabilizers. Formations of silver nanoparticles were observed visually by color change of the reaction mixture from colorless to dark yellow. Interestingly, the reaction mixture remained colorless and no absorption peak due to the Ag-nanoparticles was observed at higher [S₂O₃²⁻] ($\geq 20.0 \times 10^{-4}$ mol dm⁻³). UV-vis spectroscopy and transmission electron microscopy (TEM) were used to monitor the growth and morphology of Ag-nanoparticles, which reveal to the nano nature of the particles. These studies infer that the particles are mostly spherical in shape and have an average size of 16 nm in absence of CTAB. Selected area electron diffraction (SAED) results indicate that the Ag-nanoparticles grow along the [111] direction.

Keywords: Sculpturing effects; Silver nanoparticles; Etching agent; thiosulphate

1. INTRODUCTION

Sodium thiosulfate is used as a photographic fixer, known as "Hypo" to prevent the chemicals of photographs from further getting dark and fix the pictures, much like a preservative, from preventing the pictures to be developed from further chemical oxidation [1]. Thiosulfate ions are stable in alkaline solution but disproportionate to colloidal suspension of S and SO₃²⁻ ion in acidic medium. Silver metal is also used in electrical contacts and conductors, in mirrors and in catalysis of chemical reactions. Its compounds are used in photographic film, and dilute silver nitrate solutions and other silver compounds are used as disinfectants and microbiocides. The reaction that occurs is referred to as

fixing; it involves of complex ion formation to bring AgBr in solution. The terminal sulfur atom in $S_2O_3^{2-}$ binds to soft metals with high affinity. Thus, silver halides, e.g. AgBr, typical components of photographic emulsions, dissolve upon treatment with aqueous thiosulfate. The reactions in fixing can be written as follows:



It is known that treatment of silver chloride/ or nitrate with solutions of sodium thiosulfate or ammonium, as a rule, results in the formation of water soluble complex compounds: $Na_3[Ag(S_2O_3)_2](aq)$ or $[Ag(NH_3)_2]Cl(aq)$.

Long silver nanowires (lengths of more than 50 μm and average diameters of about 80 nm) were synthesized by a simple and fast process derived from the development of photographic films at room temperature [2]. Bokhonov deposited the platinum on the outer surface of carbon-encapsulated silver nanoparticles by adding an ammonia or sodium thiosulfate solutions [3]. Liu et al. reported the sculpturing effect of sodium thiosulfate in shape transformation of silver nanoparticles from triangular nanoprisms to hexagonal nanoplates and suggested thiosulfate etched the corners of the triangular silver nanoprisms [4]. Lengke and Southam [5] prepared the cubic gold nanoparticles by sulfate-reducing bacteria cultured in the presence of gold(I)- thiosulfate complex in aqueous solution and discussed the mechanism of reduction processes. Xu and his coworkers [6] have discussed sculpturing effect of chloride ions in shape transformation from triangular to discal silver nanoplates. Chaudhuri and Paria synthesized the sulfur nanoparticles by an acid catalyzed precipitation of sodium thiosulfate in presence of different surfactant and discussed the effect of cationic, anionic and nonionic surfactants on particle size. Surfactant significantly reduced the particle size without changing the shape and size reducing ability depending on the type of surfactant [7].

Silver nanoparticles are currently being utilized in several technological applications and are gaining popularity as a form of counter measures against several illnesses that cannot be treated through conventional means and have several characteristics that make it currently among the most widely used nanoparticle in science [8-15]. Silver nanoparticles have unique optical properties because they support surface plasmons. Any visible change to the color of the nanoparticles in solution typically indicates that the aggregation state of the nanoparticles has changed [16,17]. Generally, various stabilizers (surfactants, gemini surfactants, polymers, triblock polymers, proteins and carbohydrates) have been used in the synthesis and characterization of different shaped and sized of advanced silver nano materials [18, 19]. Eastoe et al. [20] synthesized gold and gold-palladium nanoparticles in mixed reverse micelles and used as oxidation catalysts. These investigators also suggested that the nanoparticles could be recovered and re-dispersed by tuning solvent quality.

Selection of solvent medium, environmentally benign reducing agent and suitable stabilizers for the nanoparticles stability are the main steps based on green chemistry perspectives [19]. The formation of silver nanoparticles from the reduction of Ag^+ ions with thiosulfate has not been investigated so far. Thus, the goal of this study was to investigate the interaction between silver nitrate and thiosulfate with or with out stabilizers. For this purpose, we used two stabilizers (one surfactant and one polymer), namely, cetyltrimethylammonium bromide and poly(vinyl)alcohol). Incidentally, this study appears to be the first report on the formation, aggregation, and shape transformation (from

nanorods to hexagonal nanoplates) of Ag-nanoparticles in presence of CTAB and PVA. The results presented in this paper will be an ignited clue for the sculpturing effects of stabilizers and would be useful for future development in the photography.

2. MATERIALS AND METHOD

2.1. Materials

The all chemicals (silver nitrate, sodium thiosulfate, $\text{Na}_2\text{S}_2\text{O}_3 \cdot 5\text{H}_2\text{O}$, poly(vinyl alcohol), PVA and cetyltrimethylammonium bromide, CTAB all BDH and Fluka 99.9%, product) were used as received. Double distilled (first time from alkaline permanganate), CO_2 -free, and deionized water were used as solvent for the preparation of stock solutions of all the reagents. Silver nitrate solution was stored in a dark glass bottle. Stock PVA solutions were prepared by slow stepwise addition of PVA to deionized water whilst rapidly stirring to avoid the aggregation of PVA. Surface tension versus $\log[\text{CTAB}]$ plots were used to check the purity of CTAB [21].

2.2. Preparation of silver nanoparticles and instrumentations

For the preparation of silver nanoparticles, a series of experiments were carried out under different experimental conditions (Ag^+ + thiosulfate, Ag^+ + CTAB + thiosulphate and Ag^+ + PVA + thiosulfate) at room temperature, i.e., 30°C . The formation of silver nanoparticles were monitored by using a UV/Vis spectrophotometer (UV-260 Shimadzu, with 1cm quartz cuvettes) to follow the appearance of the surface resonance plasmon (SRP) band in the vicinity of 325-550 nm as a function of time at 30°C , characteristic of silver nanoparticles having different morphologies (size, shape and the size distributions). An Accumet, Fisher Scientific digital pH meter 910 fitted with a combination electrode was used for pH measurements. Transmission electron microscope (JEOL, JEM-1011; Japan) was used to determine the morphologies of the silver nanoparticles, For TEM measurements, samples were prepared by placing a drop of working solution on a carbon-coated standard copper grid (300 mesh) operating at 80 kV.

2.3. Critical micelle concentration (CMC) determination

The conductometric technique was used to determine the CMC values of CTAB solutions under different experimental conditions, i.e., CTAB only, CTAB + thiosulphate and CTAB + silver nitrate. The values were determined from plots of the specific conductivity versus $[\text{CTAB}]$. The break point of nearly two straight-line portions in the plot are taken as an indication of micelle formation and this corresponds to the CMC of surfactant [22] and the values were found to be 1.01, 0.88 and 0.89 mmol dm^{-3} for water + CTAB, CTAB + thiosulfate ($0.40 \text{ mmol dm}^{-3}$) and CTAB + silver nitrate ($0.40 \text{ mmol dm}^{-3}$), respectively, at 30°C .

3. RESULTS AND DISCUSSION

3.1. Characterization of Silver nanoparticles in absence of stabilizers

It is well known that stability of sodium thiosulfate and metal nanoparticles depends strongly on the pH of the working solution and growth of nanoparticles can be stopped by adding the small

amounts of minerals acids [23]. In an acidic solution, sodium thiosulfate undergoes through a disproportionation reaction to sulfur and sulfonic acid (Eq.2).



On the other hand, silver thiosulfate, $\text{Ag}_2\text{S}_2\text{O}_3$, is an insoluble precipitate formed when a soluble thiosulfate reacts with an excess of silver nitrate. In the presence of excess thiosulfate, the very soluble $\text{Ag}_2(\text{S}_2\text{O}_3)_3^{4-}$ and $\text{Ag}_2(\text{S}_2\text{O}_3)_5^{6-}$ complexes form [24]. Therefore, stoichiometric ratio of Ag^+ / $\text{S}_2\text{O}_3^{2-}$ and control of pH are the crucial problem to obtain the perfect transparent silver sol that we address first. The flask containing silver nitrate and thiosulfate solutions showed gradual change in color of reaction mixture from colorless to characteristic dark yellow color with intensity increasing during the reaction time confirming the formation of Ag^0 nanoparticles [25]. The negative control (pure thiosulfate and/or silver nitrate solution) did not show the characteristic change in color also suggesting that the synthesis is not a thermal and temporal process.

To confirm the nature of yellow color, the spectrum of reaction mixture was recorded at different time intervals (Fig.1). The most characteristic part of silver sol is a narrow surface plasmon resonance absorption band observable in the 350–600 nm regions. Interestingly, our spectra of resulting silver nanoparticles showed a large band covering the whole visible region of the spectrum. In order to obtain insight into the nature of sol, the Rayleigh's law (absorbance = concentration / wavelength) was also used. The plot of log (absorbance) versus log (wavelength) is linear with slope = -5.2 (Fig. 1; inset). It is well known that if the yellow color is due to the formation of colloidal silver particles, the spectrum will be mainly due to the scattering of light (Rayleigh's law) [26, 27]. Thus, we may safely conclude that the available data are consistent with the formation of colloidal silver nanoparticles during the reduction of Ag^+ ions by thiosulfate under the present experimental conditions.

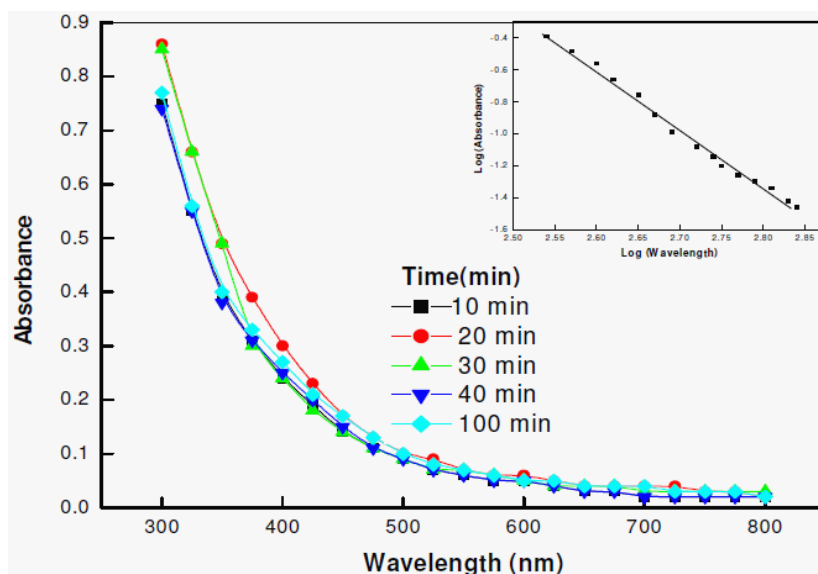


Figure 1. Absorption spectra of perfect transparent yellow colored silver nanoparticles as a function of time. *Reaction conditions:* $[\text{Ag}^+] = 0.40 \text{ mmol dm}^{-3}$, $[\text{S}_2\text{O}_3^{2-}] = 0.40 \text{ mmol dm}^{-3}$, Temperature = 30°C . Inset- plot of log (absorbance) versus log (wavelength).

Figure 2A, B, C and D shows representative low magnification, high-resolution TEM images and selected area electron diffraction (SAED) of crystalline silver nanoparticles. Fig. 2a composed of typical morphology (round irregular shaped particles and some nanorods) of Ag-nanoparticles. Fig. 2a shows a typical TEM image of these nanorods with diameters in the range of 60–80 nm. Their grain sizes measured from the micrograph range from ≤ 6 nm to 40 nm, and the mean grain size is 16 nm. Nanoparticles have clear borders, illustrating that they are well crystallized.

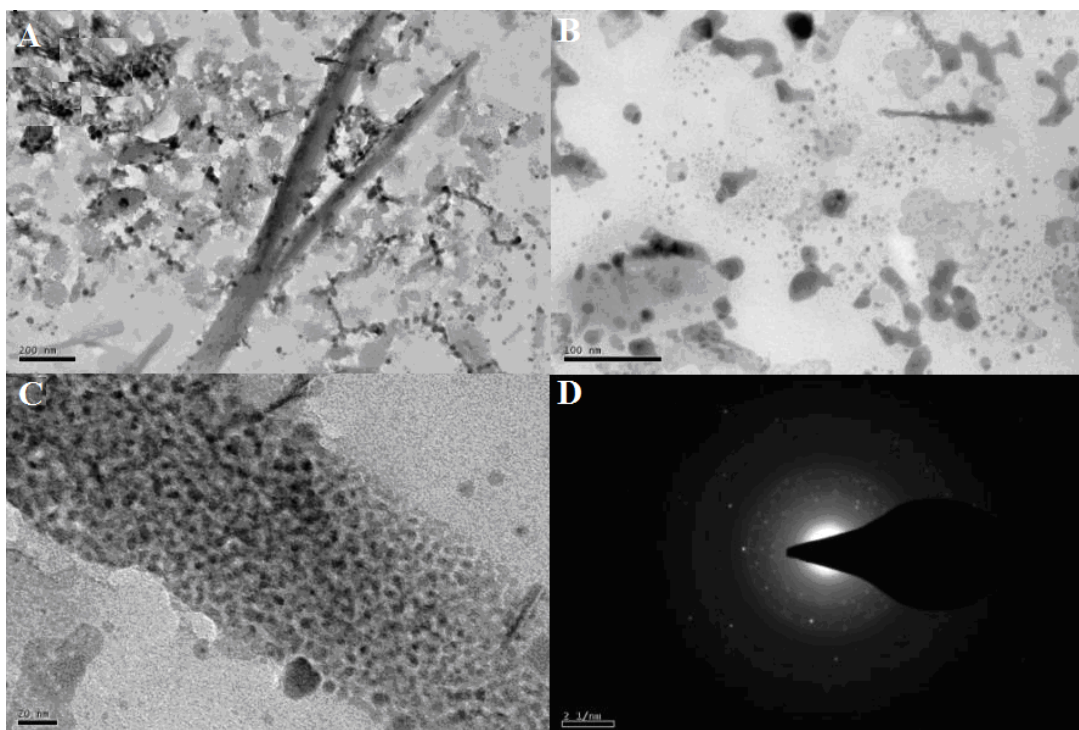


Figure 2. TEM images of silver nanoparticles. *Reaction conditions:* $[Ag^+] = 0.40 \text{ mmol dm}^{-3}$, $[S_2O_3^{2-}] = 0.40 \text{ mmol dm}^{-3}$, Temperature = 30°C .

The high-resolution images (Fig. 2c) obtained from such nanoparticles clearly show the presence of small grains of Ag-nanocrystals which are arranged in the proper way leading to the formation of nanorods (diameter = 10 nm) which matches well with the [111] crystalline plane of the metallic Ag. The lattice fringes pattern observed in the SAED images (Fig. 2D) obtained from different areas of the nanorods suggest that the nanorods is single crystalline cubic silver with a growth direction along the [111] vector [2] long silver nanorods were obtained in good yields by application of a mild reducing agent in the presence of silver nitrate.

3.2. Effect of stoichiometric ratio on the stability of silver sol

Visual observation showed that the typical color of silver nanoparticles changed from dark yellow, yellow, pale yellow, to colorless, which indicated the nanoparticle morphology altering with the molar ratio of $Ag^+ / S_2O_3^{2-}$ at different reaction stage (Table 1) and was confirmed by UV-visible spectroscopy. The position of the surface resonance plasmon absorption band and shape of the spectra strongly depends on the shape, size, dielectric constant of the surrounding medium and surface-

adsorbed species. We point out that no changes occurred in the shape of visible spectra with time in absence (Fig. 1) and presence of stabilizer, PVA (*vide infra*), support the formation of mainly one-shaped Ag-nanoparticles [19].

Table 1. Effects of $[Ag^+]$, $[S_2O_3^{2-}]$ and $[CTAB]$ on the visual appearance of silver sols

$10^4[Ag^+]$ (mol dm ⁻³)	$10^4[S_2O_3^{2-}]$ (mol dm ⁻³)	$10^4[CTAB]$ (mol dm ⁻³)	Visual observations
4.0	4.0	0	dark yellow
	8.0		yellow
	12.0		light yellow
	16.0		no color
8.0	2.0	0	yellow precipitate
	4.0		dark yellow
	8.0		yellow
	12.0		yellow
	16.0		light yellow
4.0	4.0	4.0	no color
		6.0	yellow turbid
		8.0	yellow turbid
		10.0	yellow turbid
		15.0	yellow turbid
		20.0	yellow turbid
12.0	4.0	4.0	dark yellow
		8.0	dark yellow
		10.0	dark yellow
16.0	4.0	4.0	dark yellow
		6.0	dark yellow
		8.0	dark yellow
10.0	2.0	10.0	light yellow unstable
14.0	2.0		yellow stable
18.0	2.0		yellow stable
20.0	2.0		dark yellow
24.0	2.0		dark yellow

In the first set of experiments, the effect of the ratio of thiosulfate to silver ions was investigated by measuring color at a single pH (= 6.8), varying the thiosulfate concentration but keeping the concentration of silver ions constant. Surprisingly, yellowish-white precipitate was formed instead of perfect transparent yellow color at a particular concentrations of $[Ag^+]$ (0.8 mmol dm⁻³) and $[S_2O_3^{2-}]$ (0.2 mmol dm⁻³), indicating the formation of insoluble $Ag_2S_2O_3$ in excess of Ag^+ ions. Table 1 showed a strong dependence of color and stability of silver nanoparticles on the ratio of thiosulfate to silver. The solution of silver nitrate (0.8 mmol dm⁻³) turned dark yellow after the addition of thiosulfate (0.4 mmol dm⁻³). The resulting transparent silver sol is stable at room temperature stored in a transparent vial as long as one week. Table 1 data covering a wider range of reactants concentrations (effects of $[Ag^+]$, $[S_2O_3^{2-}]$ and $[CTAB]$) confirm that path of the silver nanoparticles formation has

complicated features. In the second set of experiments, the most important and interesting findings of the present observations are the decrease in the absorbance of silver nanoparticles with $[\text{S}_2\text{O}_3^{2-}]$ from 0.4 to 1.6 mmol dm^{-3} at fixed $[\text{Ag}^+] = 0.4 \text{ mmol dm}^{-3}$ (Fig. 3). On the other hand, at higher $[\text{S}_2\text{O}_3^{2-}]$ ($\geq 2.0 \text{ mmol dm}^{-3}$), reaction mixture became colorless; instead of yellow colored silver nanoparticles due to the formation of soluble $\text{Ag}_2(\text{S}_2\text{O}_3)_3^{4-}$ and $\text{Ag}_2(\text{S}_2\text{O}_3)_5^{6-}$ complexes in excess of thiosulphate [24].

The different roles of thiosulfate may be explained in terms of the adsorption of (although highly schematic) on the surface of silver nanoparticles (Scheme 1).

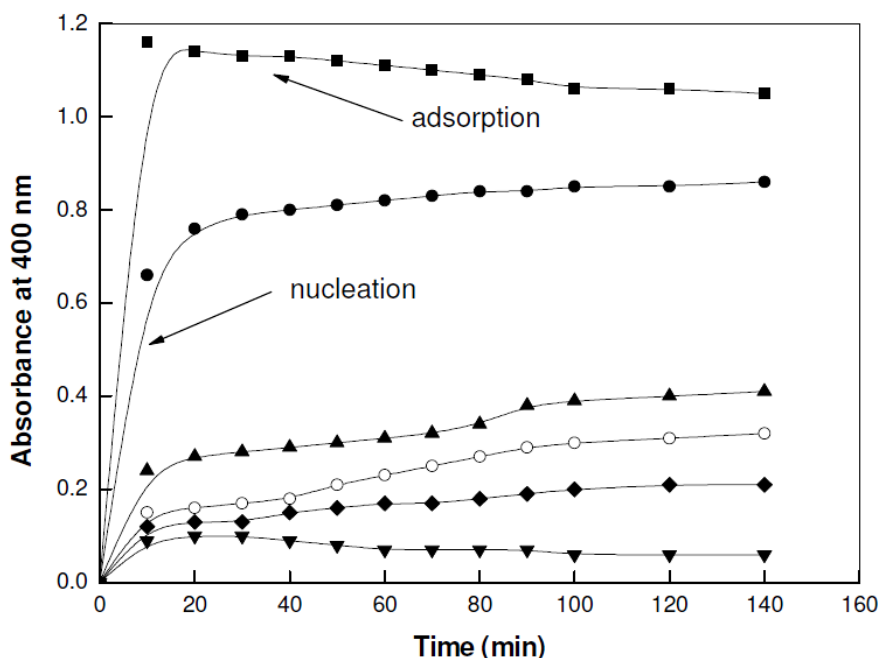
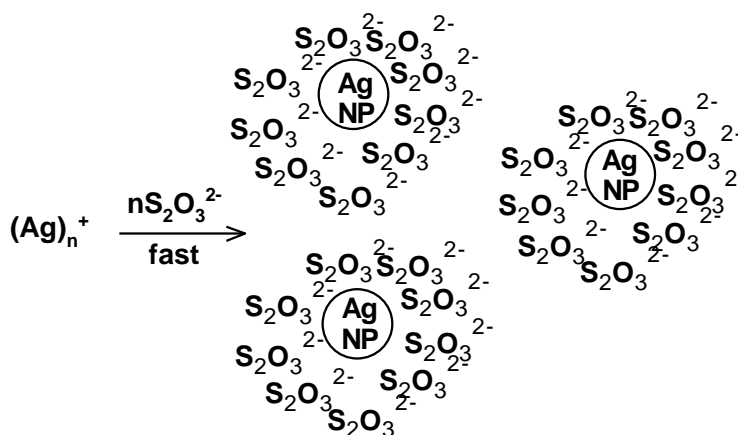


Figure 3. Reaction-time plots to the formation of Ag-nanoparticles as a function of $[\text{S}_2\text{O}_3^{2-}]$ at 30°C . Reaction conditions: $[\text{Ag}^+] = 0.80 \text{ mmol dm}^{-3}$, $[\text{S}_2\text{O}_3^{2-}] = 0.60$ (■), 0.80 (●), 1.0 (▲), 1.2 (○), 1.4 (◆), and 1.6 mmol dm^{-3} (▼).



Scheme 1. Adsorption of thiosulfate on the surface of silver nanoparticles

The adsorbed $\text{S}_2\text{O}_3^{2-}$ etched the surface of the silver nanoparticles, the Ag^0 atoms that were removed aggregated into small clusters and also causes the removal of Ag^+ ions from the surface of $(\text{Ag})_n^+$ by forming the water-soluble complex of sodium dithiosulfatoargentate which was followed by its hydrolysis and subsequent dissociation of Ag atoms to form stable Ag_2S [24, 28]. The role of

thiosulfate observed under the present experimental conditions (Table 1) is in agreement with results of Solomon et al. [29] and Li et al. [4] on the breakdown (instability) of silver nanoparticles in excess of sodium borohydride and etching effect of thiosulfate on the corner of the triangular silver nanoprisms.

3.3. Sculpturing effects of CTAB on the morphology of silver nanoparticles

Chen et al. [30] reported on the silver plate seeded synthesis of gold monopods, bipods, tripods, and tetrapods using the CTAB as a capping agent. Generally, a surfactant (e.g., cetyltrimethylammonium bromide) is required as a shape-directing agent in the syntheses of branched metal nanostructures of noble metals by preferential adsorbing on specific crystal planes [31]. The choice of an appropriate surfactant is highly important to obtain monodisperse noble metal nanoparticles [32]. In order to gain deeper understanding of the growth mechanism of the silver nanorods, a series of experiments with systematically varied reaction conditions was conducted. Different stoichiometric ratios of $[Ag^+]$ and $[S_2O_3^{2-}]$ were used to examine the effect of CTAB concentrations at below and above the CMC (*vide supra*). The observations are summarized in Table 1. CTAB stabilized the silver nanoparticles to form stable aqueous solutions, the color of which changed from pale yellow to yellow with the increase in the molar ratio of the reactants (Table 1). Under careful observation, it is noted that the molar ratio of $CTAB/[Ag^+]$, $CTAB/[S_2O_3^{2-}]$ and $[Ag^+]/[S_2O_3^{2-}]$ played multiple roles (moderator, shape controller and stabilizing agent) in the formation of perfect transparent, dark yellow color and stable silver sol. As shown in Table 1, in increase in the molar ratio of reductant, oxidant and stabilizer led to a morphology evolution of silver nanoparticles.

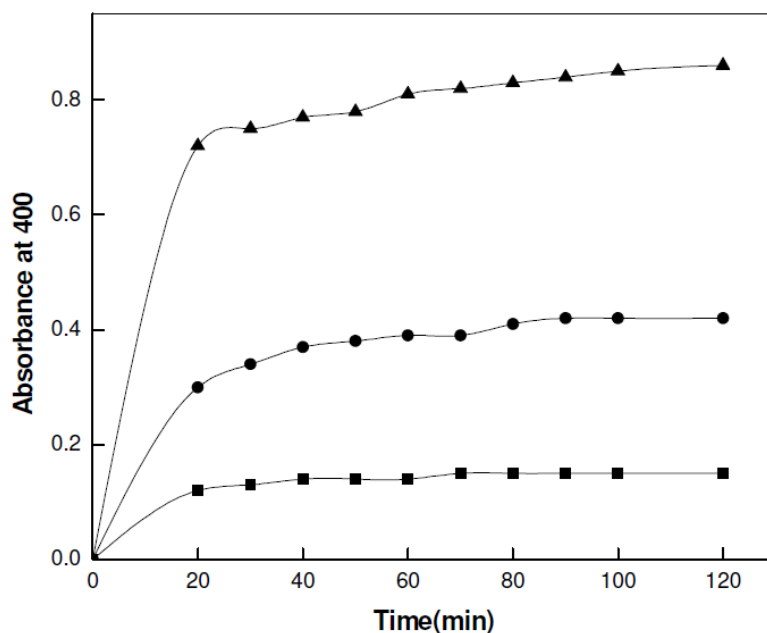


Figure 4. Reaction-time plots to the formation of silver nanoparticles in absence (■) and presence of stabilizers (PVA = ● and CTAB = ▲). Reaction conditions: $[Ag^+] = 0.80 \text{ mmol dm}^{-3}$, $[S_2O_3^{2-}] = 0.80 \text{ mmol dm}^{-3}$, $[PVA] = 2.0 \text{ mmol dm}^{-3}$, $[CTAB] = 1.0 \text{ mmol dm}^{-3}$, Temperature = 30°C .

Sigmoidal shape of the curves, as shown in Fig. 4, (plots of absorbance versus time) clearly suggests that autocatalysis was involved in the path of silver nanoparticles formation [33]. Fig. 4 clearly indicates that the formation of silver nanoparticles was found to be independent on the reaction time (Fig. 4A) and growth processes was not observed in the absence of stabilizers whereas time is an important parameter for the growth of silver nanoparticles in presence of stabilizers (CTAB (B) and PVA(C)). Inspections of these results suggesting that shape of the each reaction-time curves strongly depend on the nature of stabilizers present in the reaction mixture at the beginning to the nucleation process. The observed images are given in Fig. 5. The size of each Ag- particle is ranging from less than 4 to 15 nm. The high-resolution TEM images suggested that the resulting sol has a variety of shapes: sphere, hexagonal, triangle and irregular with broader size distribution (Fig. 5B). Interestingly, no nanorods were detected in presence of CTAB.

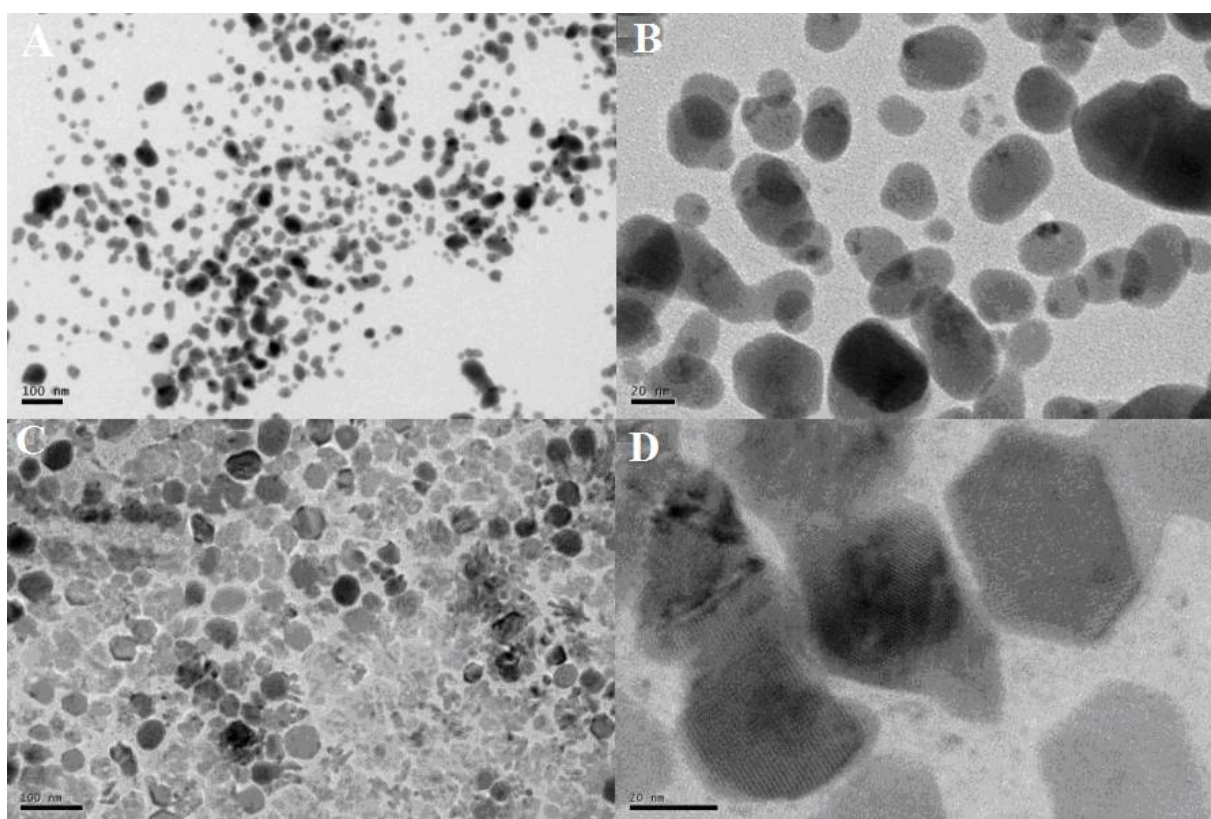


Figure 5. TEM images of silver nanoparticles in presence of CTAB = 1.0 mmol dm^{-3} (A and B) and PVA = 1.0 mmol dm^{-3} (C and D) only. Reaction conditions: $[\text{Ag}^+] = 0.40 \text{ mmol dm}^{-3}$, $[\text{S}_2\text{O}_3^{2-}] = 0.40 \text{ mmol dm}^{-3}$, Temperature = 30°C .

3.4. Sculpturing effects of PVA on the morphology of silver nanoparticles

Fig. 5 C and D shows the TEM image of the Ag- nanoparticles, which are composed mainly of hexagonal shaped particles in presence of PVA. Their grain sizes measured from the micrograph range from 25 nm to 80 nm, and the mean grain size is 42 nm. Hexagonal plate-like Ag-nanoparticles have clear borders. The reasons for this change of morphology from nanorods to spherical and

hexagonal, respectively, in the absence and presence of stabilizers (CTAB and PVA) are not understood and may be due to interactions such as hydrogen bonding and electrostatic interactions between the CTAB head group and polar carbonyl group of PVA molecules bound to the nanoparticles.

Surfactant monomers rapidly join and leave micelles (as micelles have a transient character), and the aggregation number represents only an average over time. The pre-micellar effect (Table 1) can be brought in the fact that aggregates of CTAB (dimers, trimers, tetramers, etc.) exist below the CMC, these small submicellar aggregates can interact physically with the reactants forming active entities. On the other hand, reactants incorporate in the Stern layer of CTAB micelles (most of the ionic micelle mediated reactions are believed in this region [34]) through electrostatic, hydrophobic and/or Van der Waals forces. Based on the above description, the possible cause of sculpturing effects of CTAB may be discussed. The presence of negative charge on the $S_2O_3^{2-}$ must be considered. It is certainly possible that $S_2O_3^{2-}$ forms an ion pair ($Q^+ S_2O_3^{2-}$) with the positive quaternary ammonium ($Q^+; -N^+(CH_3)_3$) head group of CTAB molecules which brings the reactants together through electrostatic interactions. Coordination of a Q^+ cation with the $S_2O_3^{2-}$ anion would decrease electron density of the $S_2O_3^{2-}$ which, in turn, increases the oxidizing power of the $S_2O_3^{2-}$. This is a reasonable explanation for the change in the morphology of Ag-nanoparticles from nanorods to nanosphere (Fig.2a and 5a). $S_2O_3^{2-}$ incorporated electro-statically into the micellar Stern layer.

Micelles exert a medium effect influencing reactivity (the effect arises from a combination of cage, pre-orientation, micro viscosity, polarity and charge effects [35 a]). The location of reactants in the micellar structure and degree of penetration of water into micellar has a major influence on reactivity. The fact is that the micellar-pseudo phase is regarded as a micro-environment having varying degrees of polarity, water activity and hydrophobicity increasing with distance from the interfacial region to its core [35b]]. Stern layer is also a water rich region because micelles are the porous cluster [35c]. Therefore, presence of Ag^+ in the reaction site can not be ruled out completely. Formation of ion-pair and/or complexation between CTAB aggregates and $S_2O_3^{2-}$ inhibits the all processes (nucleation, growth, adsorption and deposition) involved in the formation and stabilization of metal nanoparticles. We suggest a possible CTAB micellar role to explain the sculpturing effect in the formation of nanospheres. First, $S_2O_3^{2-}$ interacts with CTAB micelles to form complex, then the extra amount of CTAB might have the strong ability to solubilizing the Ag^+ ions, thus it can inhibit the electron transfer from $S_2O_3^{2-}$ to Ag^+ ions. It is also possible that Ag-nanoparticles adsorbed on the surface of CTAB molecules through Van der Waals forces and sculpturing the growth of nanorods, which is the signature of the formation of nanospheres. It is been established that the positively charged silver nanoparticles are formed due to the adsorption/complexation of Ag^+ onto the surface of Ag^0 leads to the formation of stable species of positively charged silver nanoparticles, i.e., Ag_4^{2+} [36]. Excess of $S_2O_3^{2-}$ adsorbed on the surface the resulting silver nanoparticles through electrostatic interactions (Scheme 1) to make the overall particle negative to which positively charged CTAB interacts both electrostatically and hydrophobically to form a bi-layer providing a net positive charged silver nanoparticles that is stable due to both steric and electrostatic repulsions between the particles [37]. These results are in good agreement with the observations of Sui and his coworkers on the preparation of positively charged silver nanoparticles capped by cetyltrimethyl ammonium bromide in

aqueous solution [38]. Surfactant concentration is also one important factor for the particle sizes and it seems that suitable concentrations of thiosulphate, Ag^+ ions and CTAB (above and/or below CMC) are required to the preparation of perfect transparent yellow colored and stable silver nanoparticles (Table 1). In the presence of CTAB within a suitable reactants ($\text{S}_2\text{O}_3^{2-}$ and Ag^+) concentration range spherical particles are obtained in contrast to the with out surfactants if all other conditions are remain same. These results are in good agreement with the observations of other investigators to the shape-directing role of CTAB [13, 14, 38, 39].

In presence of PVA well-shaped hexagonal silver nano-plates with an average size of 100 nm were formed. Silver ions reduced by $\text{S}_2\text{O}_3^{2-}$, and the grains metallic silver are replenished by silver ions from the solution. This could account for the here observed hexagonal nano-plates formation. These particles may be compared with those obtained directly by reduction of AgNO_3 with L-ascorbic acid in the presence of silver seeds and cetyltrimethylammonium bromide [40]. Although the role of PVA is not yet understood, it may be speculated that it serves a similar role as PVP in that it binds preferably to certain crystal faces [41]. The lone pair electrons of oxygen atoms are responsible for the adsorption of PVA on the positive surface of silver particles, which inhibit the growth, size and the reaction rate [36]. The mechanism of the hexagonal silver nanoplate formation is not yet completely understood in presence of PVA.

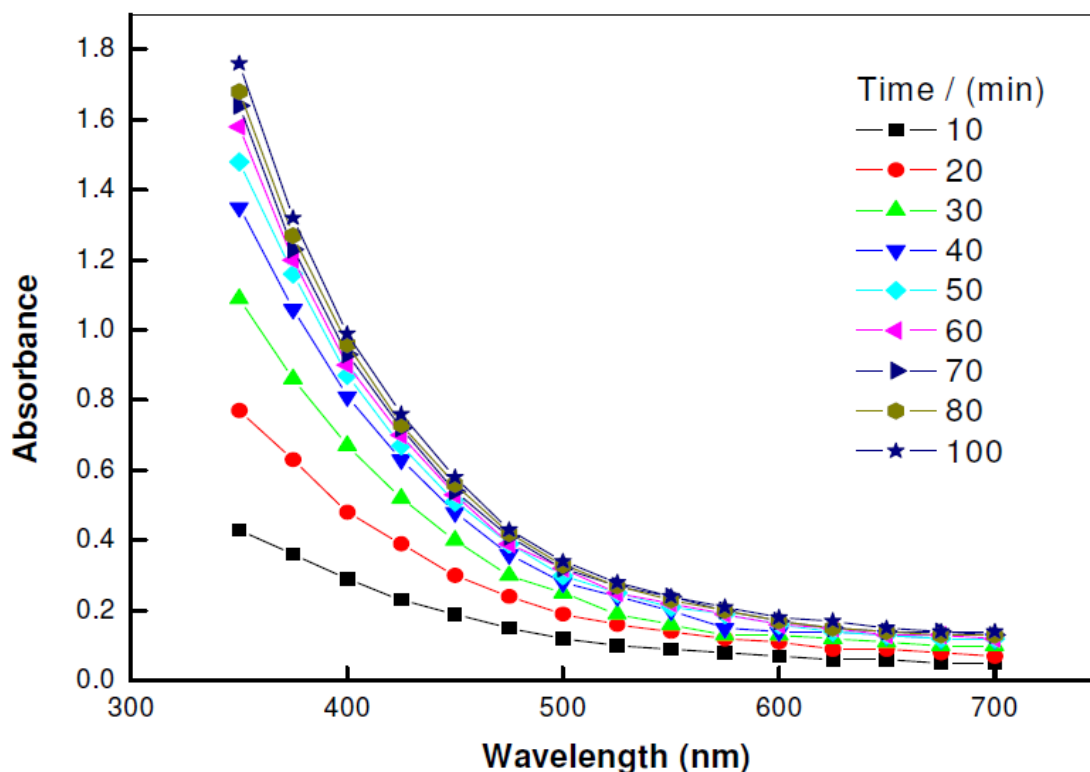


Figure 6. Absorption spectra of perfect transparent yellow colored silver nanoparticles in presence of PVA at different time intervals. *Reaction conditions:* $[\text{Ag}^+] = 1.0 \text{ mmol dm}^{-3}$, $[\text{S}_2\text{O}_3^{2-}] = 1.0 \text{ mmol dm}^{-3}$, $[\text{PVA}] = 2.0 \text{ mmol dm}^{-3}$, Temperature = 30°C .

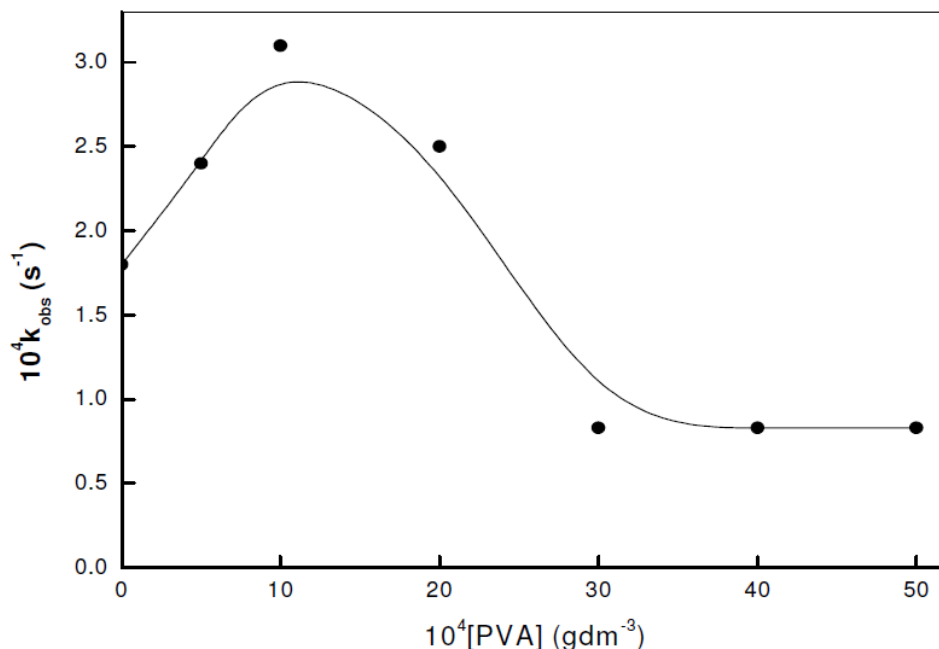
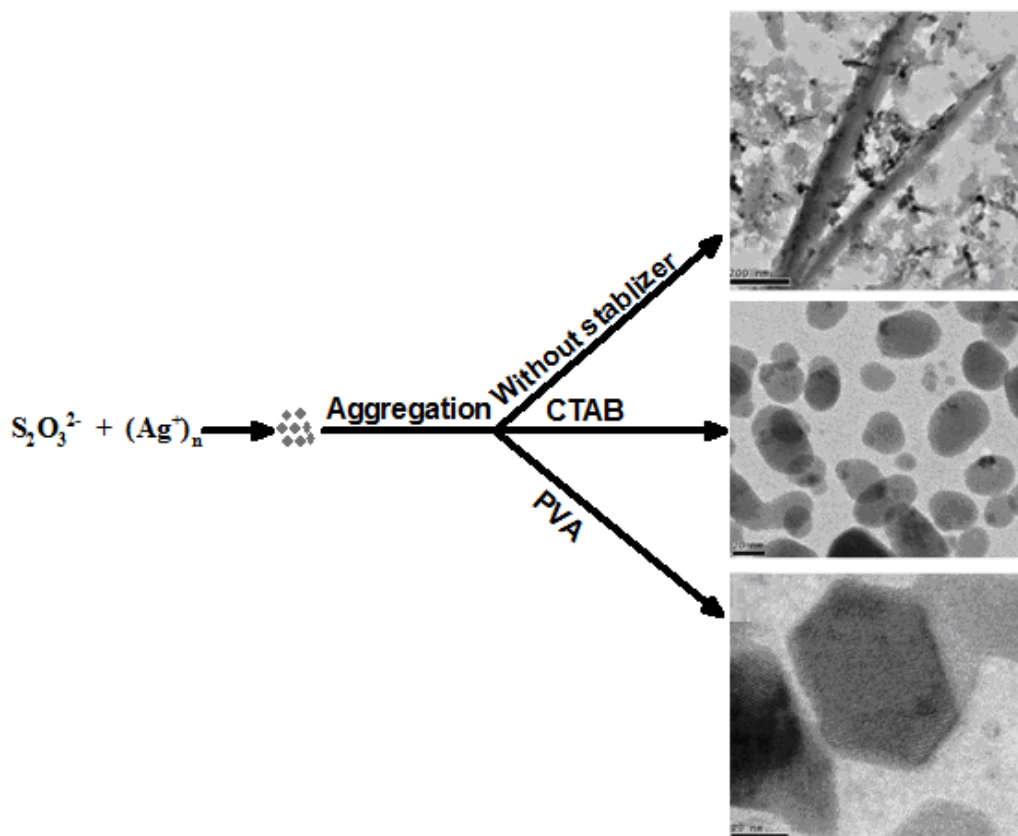


Figure 7. Effects of [PVA] on the apparent rate constants (k_{obs}) of Ag-nanoparticles. *Reaction conditions:* $[\text{Ag}^+] = 0.40 \text{ mmol dm}^{-3}$, $[\text{S}_2\text{O}_3^{2-}] = 1.0 \text{ mmol dm}^{-3}$, Temperature = $30 \text{ }^\circ\text{C}$.

However, it has now been demonstrated that the necessary requirements are at least (i) a film consisting of an emulsion of silver ions in PVA, (ii) a mild reducing agent, and (iii) the presence of silver ions in solutions. Lack of any of these ingredients does not afford any hexagonal nanoplates. Comparison of Figs 1 and 6 clearly suggests that the absorbance of Ag-nanoparticles generation became slower in presence of PVA. As a results, reaction rates also decreases with increasing [PVA]. Therefore, nucleation and further growth of the Ag-nanoparticles were delayed by the concentrated PVA. It was observed that increasing the PVA concentration the rate of silver nanoparticles formation increases first then decreases before reaching a constant low value. Presence of high concentrations of PVA decreased the nucleation rate (Fig. 7). The aggregation process along preferential directions is combined slow generation of silver atoms in the system and allows for the incorporation of resulting nanosize particles onto the larger hexagonal plates of metallic silver [42].

4. CONCLUSION

Several comprehensive studies on morphology and applications of Ag-nanoparticles have been reported in the literature [9, 11, 20, 23]. In the present study, thiosulfate was used as the reductant in the absence and presence of two stabilizers, namely, CTAB and PVA, which has not been referred yet. The stoichiometric ratios of Ag^+ and $\text{S}_2\text{O}_3^{2-}$ allow an easy overview of the formation, stability and aggregation of silver nanoparticles. The sculpturing effects of CTAB and PVA in shape transformation of silver nanoparticles are summarized in Scheme 2.



Scheme 2. Formation of rods, spherical and hexagonal plates of silver nano particles in absence and presence of stabilizers

The observed role of both stabilizers appears reasonable when compared to existing literature [18, 31]. Our results suggest that the preparation of nano-materials having a range of optical properties might be achievable through careful control over the concentration of sodium thiosulfate in solution. This approach will be utilized for applications of silver nanoparticles in the photography and study of their fixing processes. The ability of CTAB and PVA to transform the morphology, important feature of this work, of Ag-nanoparticles as observed in this study opens up the exciting possibility of developing further synthetic routes employing other stabilizers.

ACKNOWLEDGEMENT

The authors are thankful to Deanship of Scientific Research, King Abdulaziz University, Jeddah, KSA for the financial support in the form of research project (Ms. 328/130/1432).

References

1. C. R. Gibson, *The Romance of Modern Photography, Its Discovery & Its Achievements*, Seeley & Co, p. 37. (1908).
2. S. Liu, R. J. Wehmschulte, G. Lian, C. M. Burba, *J. Solid State Chem.* 179 (2006) 696.
3. B. B. Bokhonov, *Carbon* 49 (2011) 2444.
4. B. Liu, Z. Ma, K. Li, *J. Nanoscience Nanotechno.* 11 (2011) 5001.
5. M. Lengke, G. Southam, *Geochimica et Cosmochimica Acta*, 70 (2006) 3646.

6. J. An, B. Tang, X. Zheng, J. Zhou, F. Dong, S. Xu, Y. Wang, B. Zhao, W. Xu, *J. Phys. Chem. C*, 112 (2008) 15176.
7. R. G. Chaudhuri, S. Paria, *J. Colloid Interface Sci.* 343 (2010) 439.
8. S. Li, Y. Shen, A. Xie, X. Yu, L. Qiu, L. Zhang, Q. Zhang, *Green Chem.* 9 (2007) 852.
9. P. Mulvaney, *Langmuir* 12 (1996) 788.
10. S. S. Shankar, A. Rai, A. Ahmad, M. Sastry, *J. Colloid Interface Sci.* 275 (2004) 496.
11. J. Xie, J. Y. Lee, D. I. C. Wang, Y. P. Ting, *ACS Nano* 1 (2007) 429.
12. M. S. Bakshi, *Langmuir* 25 (2009) 12697.
13. M. S. Bakshi, *J. Nanosci. Nanotechnol.* 10 (2010) 1757.
14. T. K. Sau, C. J. Murphy, *J. Am. Chem. Soc.* 126 (2004) 8648.
15. A. Rafey, K. B. L. Shrivastav, S. A. Iqbal, Z. Khan, *J. Colloid Interface Sci.* 534 (2011) 190.
16. R. Jin, Y. C. Cao, E. Hao, G. S. Metraux, G. C. Schatz, C. A. Mirkin, *Nature* 425 (2003) 487.
17. Y. Sun, Y. Xia, *Science* 298 (2002) 2176.
18. (a) C. Burda, X. Chen, R. Narayanan, M. A. El-Sayed, *Chem. Rev.* 105 (2005) 1025; (b) M. Harada, Y. Inada, M. Nomura, *J. Colloid Interface Sci.* 337 (2009) 427; (c) N. R. Jana, L. Gearheart, C. J. Murphy, *Adv. Mater.* 13 (2001) 1389; (d) P. Vasileva, B. Donkova, I. Karadjova, C. Dushkin, *Colloids Surfaces A: Physicochem. Eng. Aspects*, 382 (2011) 203; (e) J. Gao, C. M. Bender, C. J. Murphy, *Langmuir* 19 (2003) 9065; (f) Z. Khan, S. A. AL-Thabaiti, A. Y. Obaid, Z. A. Khan, A. O. Al-Youbi, *J. Colloid Interface Sci.* 367 (2012) 101-108.
19. P. Raveendran, J. Fu, S.L. Wallen, *J. Am. Chem. Soc.* 125 (2003) 13940.
20. O. Myakonkaya, B. Deniau, J. Eastoe, S. E. Rogers, A. Ghigo, M. Hollamby, A. Vesperinas, M. Sankar, S. H. Taylor, J. K. Bartley, G. J. Hutchings, *J. Colloid Interface Sci.* 350 (2010) 443.
21. S.P. Harrold, *J. Colloid Sci.* 15 (1960) 280.
22. Mukherjee, P., Mysels, K.J., *Critical Micelle Concentrations of Aqueous Surfactants*, NSRDS-NBS # 36, Superintendent of Documents, Washington, DC (1971).
23. (a) B. Nikoobakht, M. A. El-Sayed, *Chem. Mater.* 15 (2003) 1957; (b) B. G. Ershov, E. Janata, A. Henglein, *J. Phys. Chem.* 97 (1993) 4589.
24. A.I. Vogel, in: G. Svehla (Ed.), *Vogel's Qualitative Inorganic Analysis*, 7th ed., Addison Wesley Longman, Singapore, 1996.
25. V. K. Sharma, R. A. Yngard, Y. Lin, *Ad. Colloid Interface Sci.* 145 (2009) 83.
26. F. Mata – Perez, J. F. Perez – Benito, *Can. J. Chem.* 63 (1985) 988.
27. F. Freeman, J. C. Kappos, *J. Am. Chem. Soc.* 107 (1985) 6628.
28. S. Pal, G. De, *Mater. Res. Bull.* 44 (2009) 355.
29. S. D. Solomon, M. Bahadory, A. V. Jeyarajasingam, S. A. Rutkowsky, C. Boritz, *J. Chem. Educ.* 84 (2007) 322.
30. S. H. Chen, Z. L. Wang, J. Ballato, S. H. Foulger, D. L. Carroll, *J. Am. Chem. Soc.* 125 (2003) 16186.
31. (a) C. H. Kuo, M. H. Huang, *Langmuir* 21 (2005) 2012; (b) X. Teng, H. Yang, *Nano Lett.* 5 (2005) 885; (c) J. D. Hoefelmeyer, K. Niesz, G. A. Somorjai, T. D. Tilley, *Nano Lett.* 5 (2005) 435.
32. (a) M. S. Bakshi, F. Possmayer, N. O. Petersen, *J. Phys. Chem. C* 111 (2007) 14113. (b) M. S. Bakshi, S. Sachar, G. Kaur, P. Bhandari, G. Kaur, M. C. Biesinger, F. Possmayer, N. O. Petersen, *Cryst. Growth Des.* 8 (2008) 1713.
33. (a) Z.-Y. Huang, G. Mills, B. Hajek, *J. Phys. Chem.* 97(1993) 11542; (b) K. Esumi, T. Hosoyo, A. Yamahira, K. Torigoe, *J. Colloid Interface Sci.* 226 (2000) 346.
34. C. A. Bunton, *J. Mol. Liq.* 72 (1997) 231.
35. (a) S. Tascioglu, *Tetrahedron*, 52 (1996) 11113; (b) F. M. Menger, J. F. Chow, *J. Am. Chem. Soc.* 105 (1983) 5501; (c) H. A. Al-Lohedan, *J. Chem. Soc Perkin Trans 2*, (1995) 1707.
36. A. Henglein, *J. Phys. Chem* 97 (1993) 5457.
37. We are thankful to one of the reviewers for suggesting this point.

38. (a) Z. M. Sui, X. Chen, L. Y. Wang, Y. C. Chai, C. J. Yang, J. K. Zhao, *Chemistry Letters* 34 (2005) 100; (b) Z. M. Sui, X. Chen, L. Y. Wang, L. M. Xu, W. C. Zhuang, Y. C. Chai, C. J. Yang, *Physica E-Low-Dimensional Systems & Nanostructures* 33 (2006) 308.
39. (a) D. Yu, V. W.-W. Yam, *J. Am. Chem. Soc.* 126 (2004) 13200; (b) D. Yu, V. W.-W. Yam, *J. Phys. Chem. B* 109 (2005) 5497.
40. S. Chen, D.L. Carroll, *J. Phys. Chem. B* 108 (2004) 5500.
41. Y. Sun, Y. Yin, B.T. Mayers, T. Herricks, Y. Xia, *Chem. Mater.* 14 (2002) 4736.
42. L. Suber, I. Sondi, E. Matijevic, D. V. Goia, *J. Colloid Interface Sci.* 288 (2005) 489.